Supporting information

High-temperature annealing enables MXene dielectric modulation for enhancing electromagnetic wave absorption and shielding

Qingtao Lv [a, b, c], Lei Ding [e], Yawen Liu [a, b], Zhiyong Su [c], Teng Zhang [b], Yudan Wang [a], Tao Wu [c, d, *], Xiaolong Wang [c, d, *], Chunhong Zhang [a, b, *]

[a] Key Laboratory of Superlight Materials and Surface Technology of Ministry of Education, College of Materials Science and Chemical Engineering, Harbin Engineering University, Harbin, 150001, P. R. China.

[b] Harbin Engineering University Yantai Research Institute, Yantai, 264006, P. R. China.

[c] Shandong Laboratory of Advanced Materials and Green Manufacturing at Yantai, Yantai, 264006, P. R. China.

[d] State Key Laboratory of Solid Lubrication, Lanzhou Institute of Chemical Physics, Chinese Academy of Sciences, Lanzhou, 730000, P. R. China.

[e] Xi'an Aerospace Chemical Propulsion Co., Ltd. Xi'an, 710025, P.R. China.

***Corresponding author:**

Address: Harbin Engineering University Yantai Research Institute, Yantai, 264006, China (C. Zhang). Shandong Laboratory of Advanced Materials and Green Manufacturing at Yantai, Yantai, 264006, China (T. Wu and X. Wang).

E-mail: zhangchunhong97@163.com (C. Zhang), wutao@licp.cas.cn (T. Wu), wangxl@licp.cas.cn (X. Wang).

Materials

Lithium fluoride (LiF, 99%), Titanium aluminum carbide (Ti_3AlC_2, 400 mesh, 95 %), 25 wt% tetrabutylammonium hydroxide (TBAOH) aqueous dispersion, ethyl acetate (EA, AR), and anhydrous ethanol were purchased from Sigma-Aldrich. Hydrochloric acid (HCl, 37 %) was purchased from Yantai Far East Fine Chemical Co. Phenolic Cyanate (C05C0400) was purchased from Yangzhou Tianqi New Material Co. The photocrosslinking components were purchased from the Lanzhou Institute of Chemical Physics, Chinese Academy of Sciences; The deionized water was produced in the laboratory.

Simulation Method:

EM simulation analysis was conducted using CST Microwave Studio 2021. First, modeling was performed based on the module's capabilities. Subsequently, the EM parameters measured by the vector network analyzer were imported into the software. The reflection loss (RL) of a 3D unit meta-structure was numerically calculated using periodic boundary conditions with the Frequency Domain Solver. Additionally, the boundary condition Z_{min} was configured as an electric wall, while Z_{max} was designated as open space. The remaining boundary conditions were established as the unit cell.

Characterization

Scanning electron microscopy (SEM, CLARA GHM) was used to analyze the samples' layered structure, surface, and cross-sectional morphology. XRD spectra of the samples were acquired using a D8 ADVANCE XRD system with Cu Kα radiation (λ = 1.5406 Å) over a scanning range of 5° to 90°; the scanning rate was 5° min^{-1}. Transmission

electron microscopy (TEM, FEI-TALOS-F200X) was used to characterize the micromorphology, crystallite spacing, and crystallite index of TiO_2. X-ray photoelectron spectroscopy (XPS, Thermo Kalpha) determined the samples' chemical state and chemical bonding. The samples were analyzed by Raman spectroscopy using a LabRam HR Evolution Raman spectroscopy system (532 nm laser emitter). The thermal stability of $Ti_3C_2T_x$ was analyzed using a thermogravimetric analyzer (TG 209 F3 Tarsus) with a heating temperature of 10 °C min^{-1} over a temperature range of 30 ~800°C. The samples' electrical conductivity was characterized at different pressures (10 MPa,14 MPa, and 18 MPa) using a resistivity tester (ST2253y). The macroscopic morphology of 3D-printed bionic superstructure samples was characterized using a fully automated 3D super depth-of-field video microscope (DVM6A). The surface water contact angle of 3D samples was determined using a contact angle tester (SDC-100).

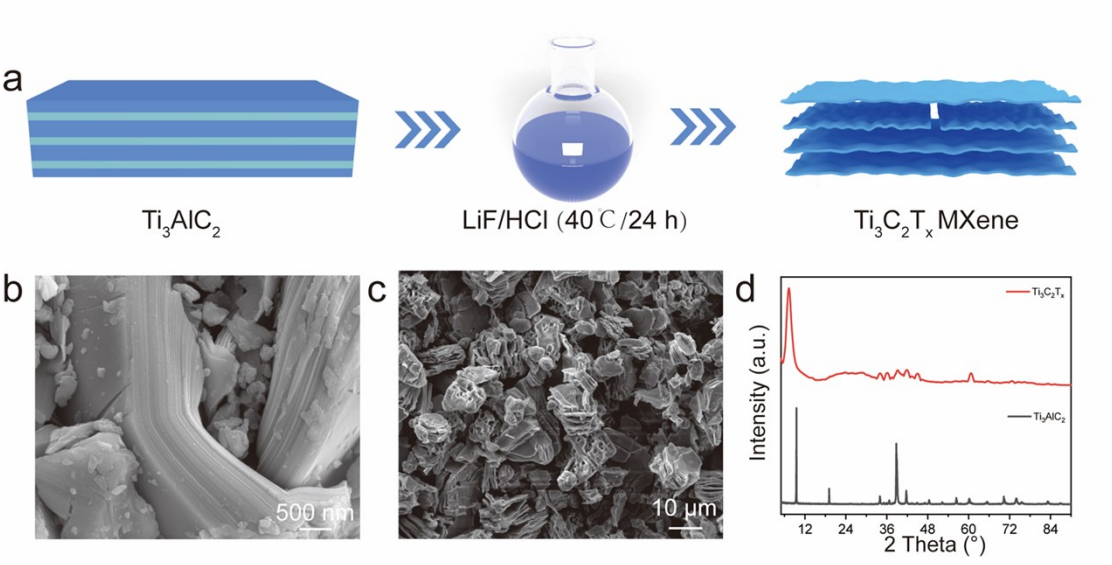

Fig. S1 Characterization of structural morphology and physical phase components of Ti_3AlC_2 before and after etching. (a) Schematic of $Ti_3C_2T_x$ MXene preparation. SEM

and TEM images of (b) Ti_3AlC_2 and (c) $Ti_3C_2T_x$ MXene. (d) XRD patterns of Ti_3AlC_2 and $Ti_3C_2T_x$ MXene.

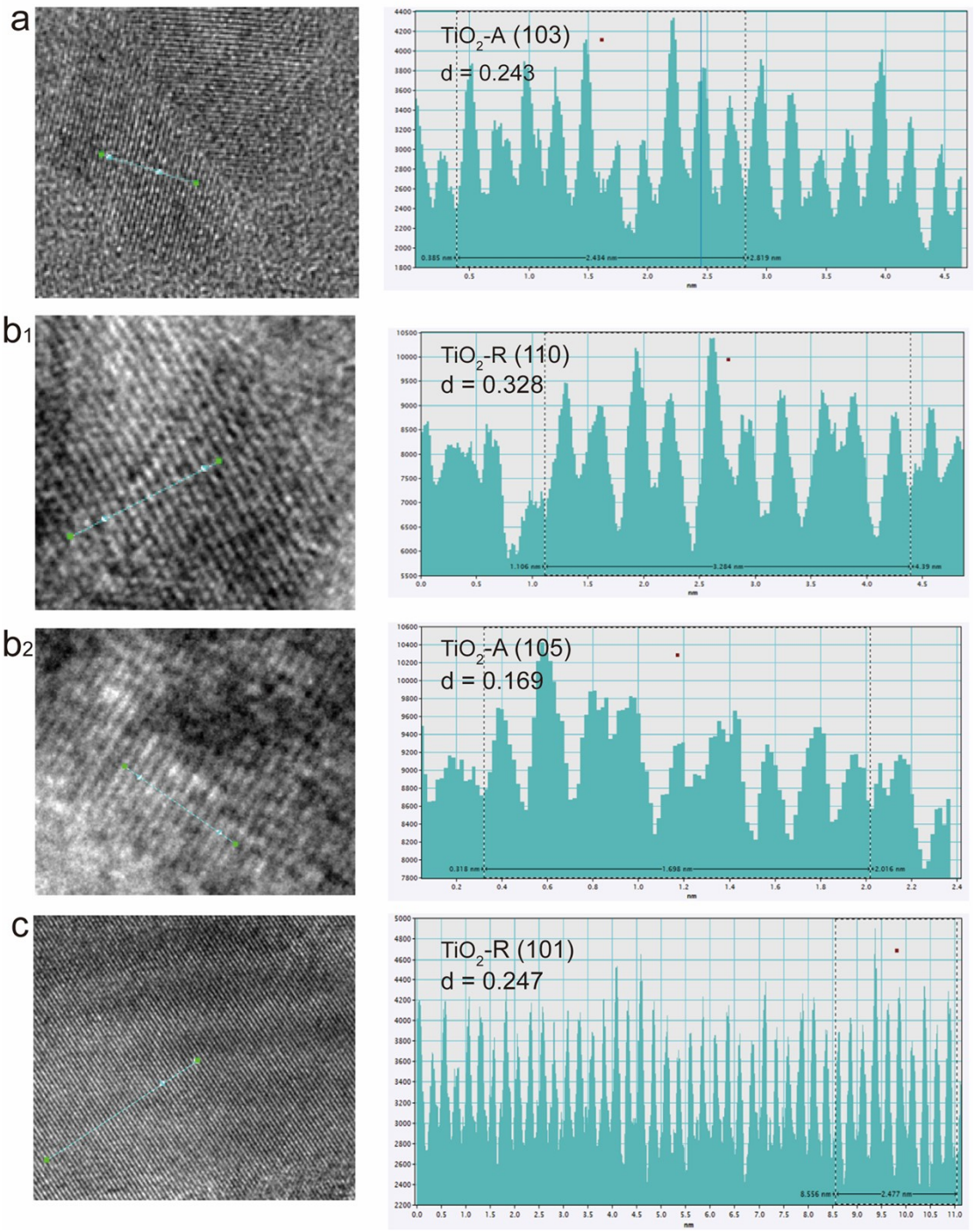

Fig. S2. a-c) HRTEM image of TiO_2-A, TiO_2-R, and the corresponding inverse fast Fourier transform (IFFT) lattice fringes are used to interpret the crystallographic indices and spacings in Figure 2.

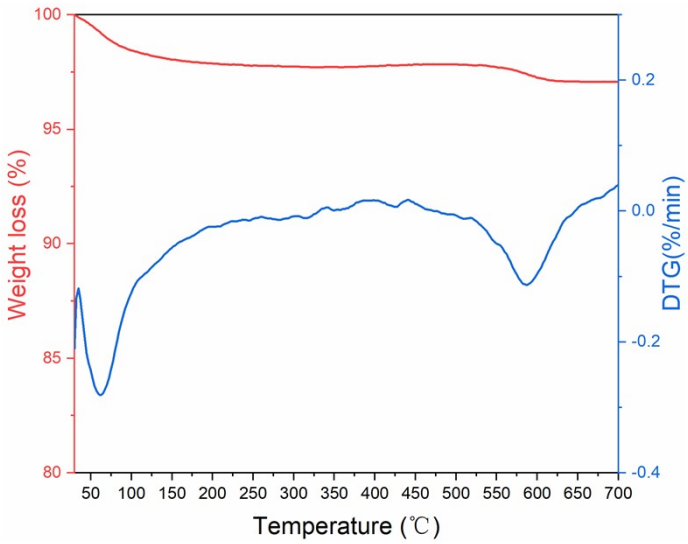

Fig. S3. TGA and DTG curves of $Ti_3C_2T_x$ MXene in N_2.

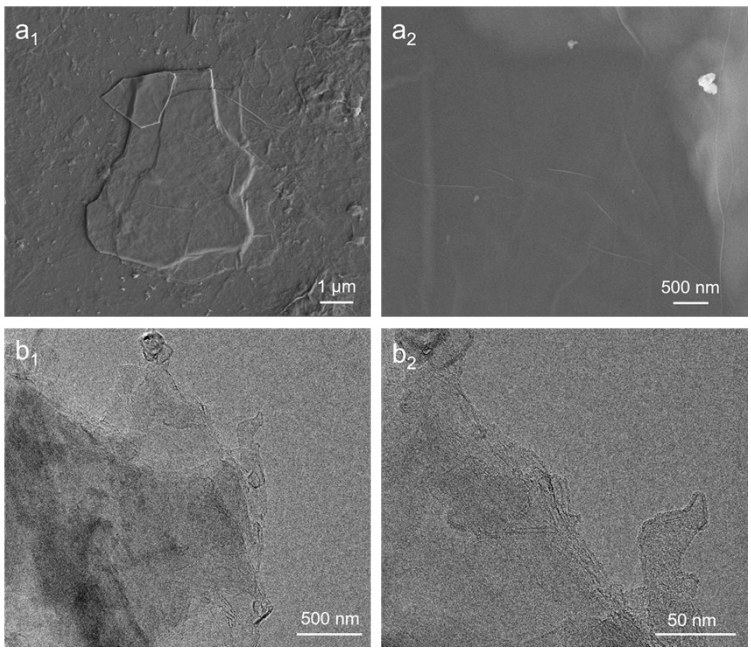

Fig. S4 a_1 and a_2) SEM, b_1 and b_2) TEM surface images of $Ti_3C_2T_x$ MXene.

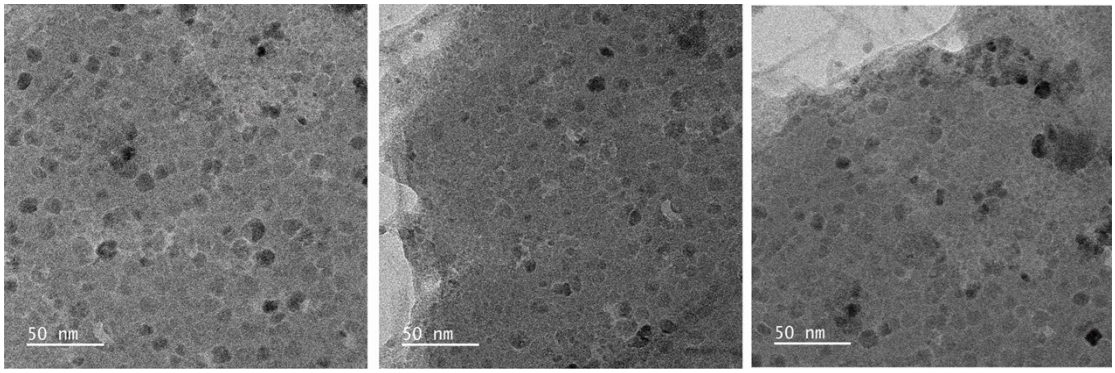

Fig. S5. TEM images of TiO_2-A-NP@$Ti_3C_2T_x$ MXene.

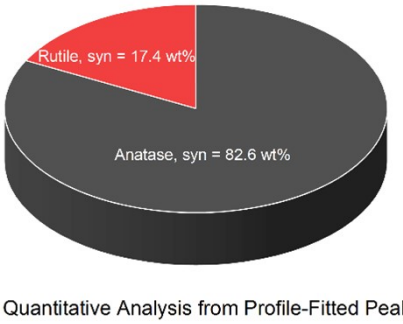

Fig. S6. The mass fraction of TiO_2-A and TiO_2-R based on the XRD pattern of the TiO_2-AR-HJ@$Ti_3C_2T_x$.

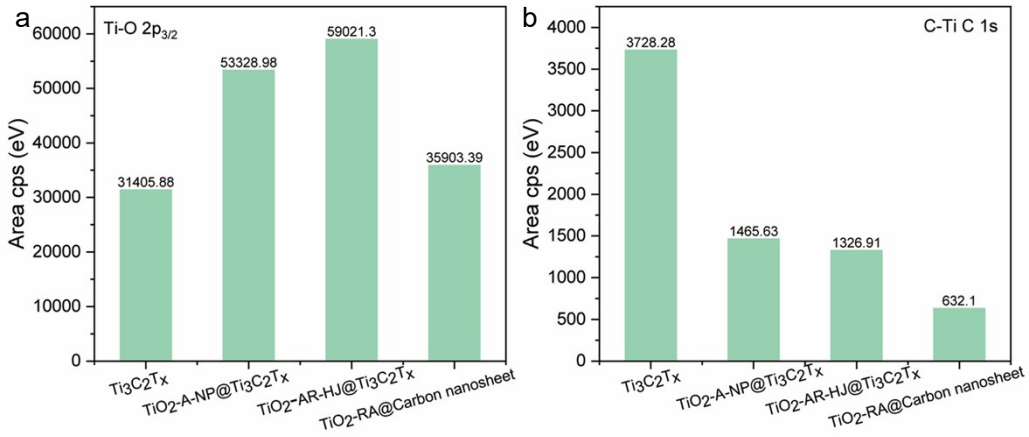

Fig. S7. The a) Ti-O $2p_{3/2}$ and b) C-Ti Area cps of $Ti_3C_2T_x$, TiO_2-A-NP@$Ti_3C_2T_x$, TiO_2-AR-HJ@$Ti_3C_2T_x$, and TiO_2-RA@Carbon nanosheet.

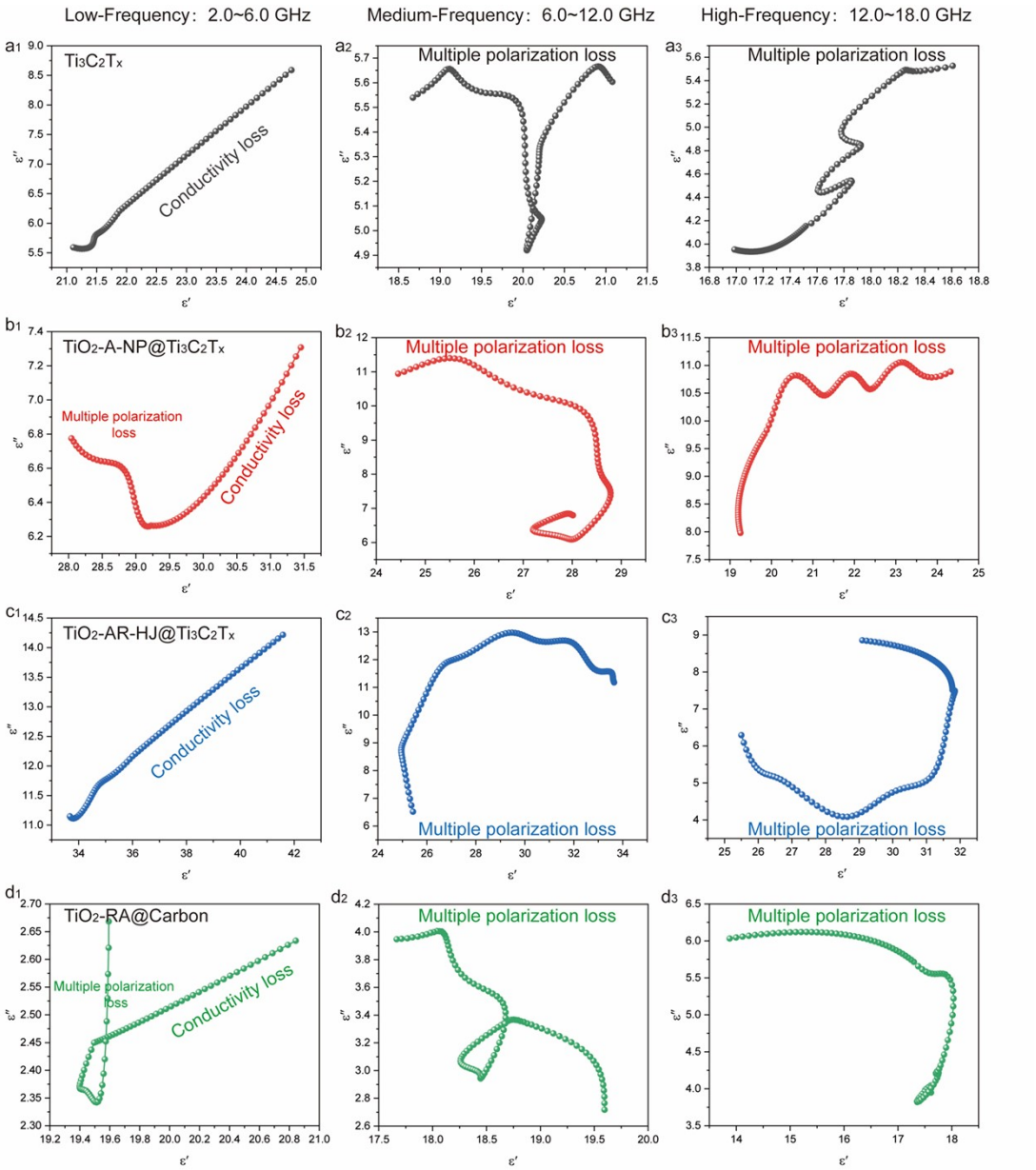

Fig. S8. Cole-Cole curves of (a_1-a_3) $Ti_3C_2T_x$, (b_1-b_3) TiO_2-A-NP@$Ti_3C_2T_x$, (c_1-c_3) TiO_2-AR-HJ@$Ti_3C_2T_x$, and (d_1-d_3) TiO_2-RA@Carbon nanosheet.

As shown in Fig. S7a_1-c_1, within the thickness range of 1.0~2.0 mm, TiO_2-A-NP@$Ti_3C_2T_x$ has the minimum reflection loss value (-37.5 dB). In contrast, TiO_2-AR-HJ@$Ti_3C_2T_x$ MXene has the maximum reflection loss value (-14.55 dB) due to the strong impedance mismatch on the surface. As shown in Fig. S7a_2-c_2, TiO_2-A-NP@$Ti_3C_2T_x$ achieves the optimal effective absorption bandwidth (4.3 GHz) at a thickness of 1.12 mm, which is attributed to the excellent impedance matching characteristics imparted to MXene by nano-TiO_2-A-NP.

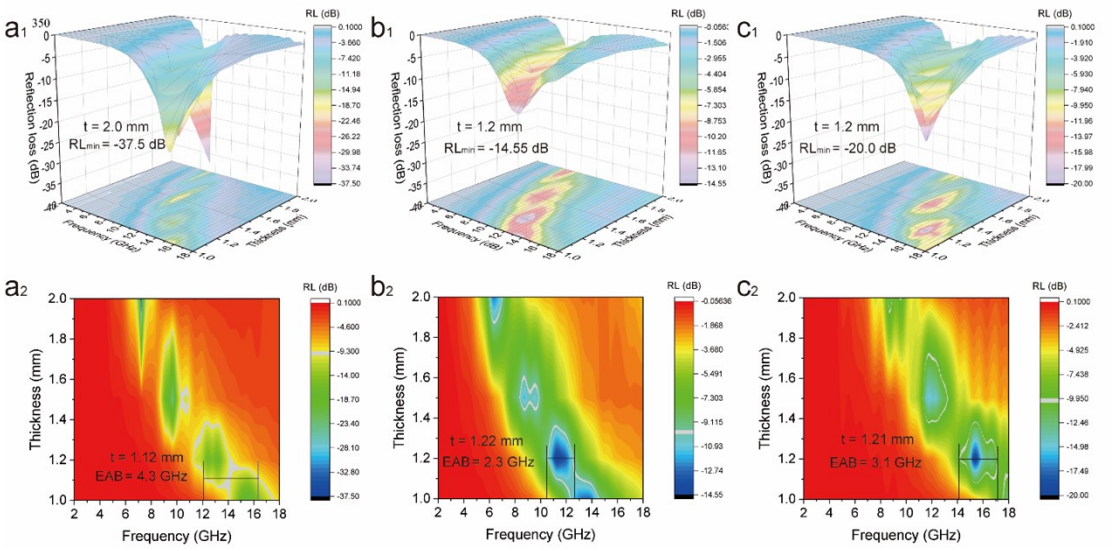

Fig. S9. a_1-c_1) 3D RL diagrams, (a_2-c_2) 2D projection images for TiO_2-A-NP@$Ti_3C_2T_x$ MXene, TiO_2-AR-HJ@$Ti_3C_2T_x$ MXene, and TiO_2-RA@Carbon nanosheet.

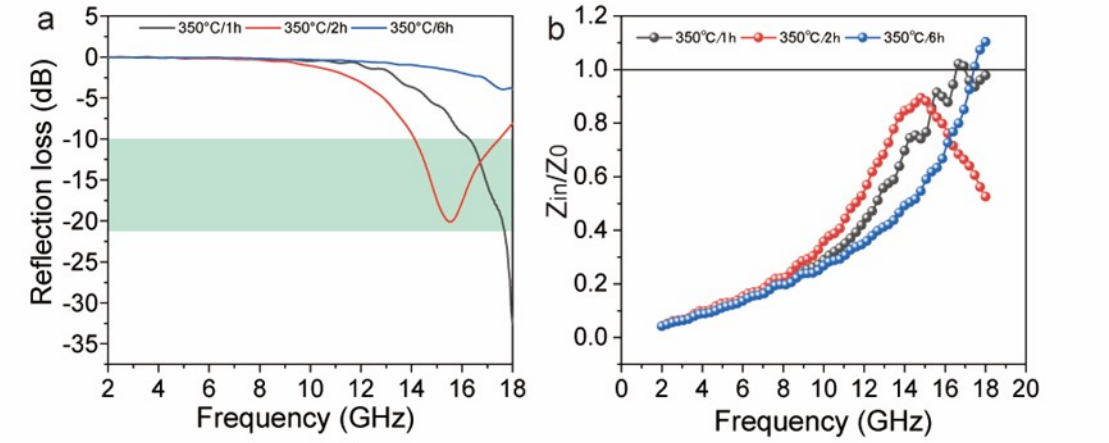

Fig. S10. The a) Reflection loss, b) Z_{in}/Z_0 of $Ti_3C_2T_x$ MXene after 350 ℃/1h, 350 ℃/2h, and 350 ℃/6h.

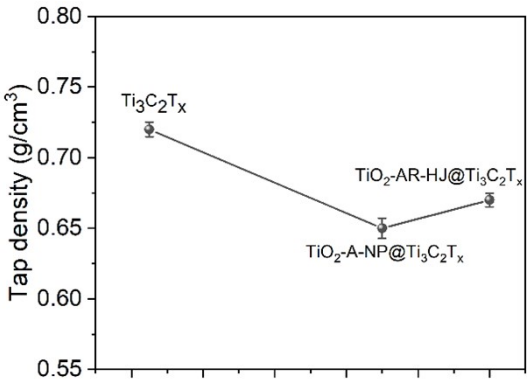

Fig. S11. The tap density of $Ti_3C_2T_x$, TiO_2-A-NP@$Ti_3C_2T_x$, and TiO_2-AR-HJ@$Ti_3C_2T_x$.

Tab. S1 The EMW absorption properties of recent similar materials.

Material Name	Matrix	Filler loading (wt%)	Thickness (mm)	EAB (GHz)	RLmin (dB)	Refs
TiO_2-A-NP@MXene	Wax	50	1.00	3.36	-20.1	This work
Nano-diamond@ MXene (MN3)	Wax	50	1.00	0.00	≈-9.90	[2]
Cl/Ni@MXene (Cl/Ni-MX-6)	Wax	40	1.00	0.00	-10.0	[3]
Co_3O_4-C@MXene	Wax	20	1.00	0.00	-2.50	[4]
$NiCoO_4$@MXene(P-MXene/$NiCo_2O_4$)	Wax	50	1.00	0.00	≈-5.0	[5]
Mesoporous MXene	Wax	7.0	1.92	2.32	-49.54	[6]
SiO_2@MXene	Wax	45	3.52	1.60	-50.11	[7]
Ni-chain@MXene (Ni-10% MXene)	Wax	10	2.0	1.80	-16.9	[8]
Network-like MXene nanoribbons (N-MXene NRs)	Wax	50	1.0	0.80	≈-10.5	[9]
MXene/amorphous carbon/TiO_2	Wax	50	1.85	2.80	-45.0	[10]
CNTs/MXene	Wax	35	2.00	3.00	-17.0	[11]
Porous MXene monolayer (P-MXene ML)	Wax	50	1.00	0.00	≈-7.00	[9]
Porous MXene layer (P-MXene ML)	Wax	50	1.00	0.00	≈-6.50	[9]

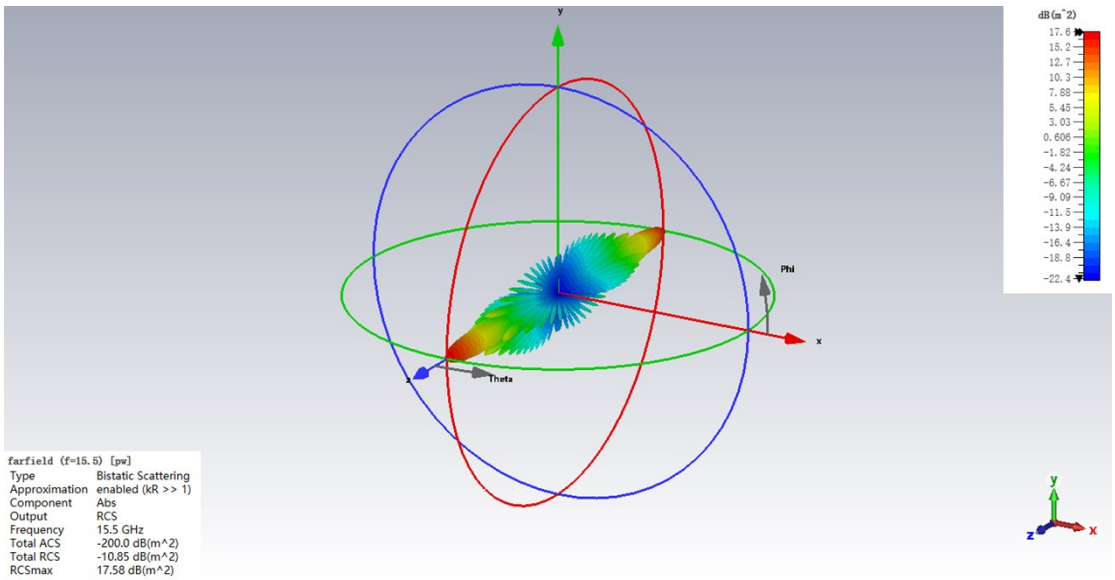

Fig. S12. The 3D RCS diagram of PEC.

Reference

[1] Q. Zhang, H. Lai, R. Fan, P. Ji, X. Fu, H. Li, *ACS Nano* 2021, 15, 5249-5262.

[2] Q. Tang, H. Jiang, F. Wu, J. Shen, *Diam. Relat. Mater.* 2024, 149, 111663.

[3] Y. He, Q. Su, D. Liu, L. Xia, X. Huang, D. Lan, Y. Liu, Y. Huang, B. Zhang, *Chem. Eng. J.* 2024, 491, 152041.

[4] Y. Hou, Z. Jia, H. Zheng, Z. Hu, L. Shen, D. Liu, L. Li, S. Liu, Y. Liu, S. Yu, *Diam. Relat. Mater.* 2024, 150, 111692.

[5] C. Zhao, X. Zeng, R. Yu, *Synthetic Metals* 2023, 297, 117402.

[6] L. Zhu, W. Wu, J. Chen, Z. Hu, J. Yu, Y. Wang, *Chem. Eng. J.* 2024, 488, 150649.

[7] R. Guo, Y. Fan, L. Wang, W. Jiang, *Carbon* 2020, 169, 214-224.

[8] L. Liang, G. Han, Y. Li, B. Zhao, B. Zhou, Y. Feng, J. Ma, Y. Wang, R. Zhang, C. Liu, *ACS Appl. Mater. Interfaces* 2019, 11, 25399-25409.

[9] X. Zeng, C. Zhao, X. Jiang, R. Yu, R. Che, *Small* 2023, 19, 2303393.

[10] M. Han, X. Yin, H. Wu, Z. Hou, C. Song, X. Li, L. Zhang, L. Cheng, *ACS Appl. Mater. Interfaces* 2016, 8, 21011-21019.

[11] X. Li, X. Yin, M. Han, C. Song, H. Xu, Z. Hou, L.Zhang, L. Cheng, *J. Mater. Chem. C.* 2017, 5, 4068-4074.